Charge Weld Scrap Minimization by Means of Dead Metal Flow Control in Die Design

Tommaso Pinter[1], Dan Antonios[2], Barbara Reggiani[3], Andrea Gamberoni[3]

[1]*Almax Mori & Alumat, Mori, Italy*
[2]*Alexandria Industries Midamerica, Indianapolis, USA*
[3]*Università di Bologna, Dipartimento di Ingegneria Industriale (DIN), Bologna, Italy*

ABSTRACT

Together with seam welds, the extrusion process involves a second type of weld generated between two consecutive billets and known as a charge or transverse weld. The scrap of the profile length marked by charge welds is crucial for extruded profiles, due to its lower mechanical properties as compared to the base material. Proper prediction and reduction of the portion to be scrapped then become mandatory, not only for the final user of the profile, in order to avoid in-service product failures, but also for extruders and die makers to increase process efficiency. The extension of the charge weld, otherwise called front-end defect, is strongly influenced and driven by the die geometry. In this context, the present work examined the dynamics of the dead metal zones in hollow extrusion dies through the use of FE analyses and looked at the effect of their minimization of the front-end defect without altering the overall process efficiency. The starting point was the industrial experimental verification of the FE model used to predict the charge weld evolution for the initial die configuration. Then, the benefits of an innovative die design approach were quantitatively evaluated by means of an extensive numerical campaign both in terms of recovery and productivity, achieving a final optimized die design that allowed the extruder to reduce the charge weld scrap. The sensitivity analysis of the results to process parameters (ram speed, billet temperature and alloy) was also performed.

INTRODUCTION

Hot aluminium extrusion is a high productivity manufacturing process widely used for many different applications ranging from civil and industrial engineering to furniture design and transportation sectors (motorbikes, automotive vehicles, trucks, trains, and aircraft). Among the properties required of an extruded product are surface appearance and tight tolerances, and proper mechanical strength all along the commercialized profile length is of crucial importance, especially in structural applications. The most common extrusion defects were previously classified and described [1]. In this work, an incorrect heat treatment, seam weld failure, and the presence of charge welds inside the profile have been identified as the most critical factors to be accurately monitored, since these were detrimental to the final mechanical properties of the profile. Both extruded bar extremities should be tested [2], since these sections are potentially corrupted by defects that affect the final profile properties: on one extremity the billet skin contamination or back-end defects [3-5]; on the other, the charge welds (front-end defects).

The charge welds, also called transverse welds, are generated when multiple billets are consecutively extruded one after the other in order to generate a continuous output profile. However, at the end of each process stroke, when a new billet is loaded into the press, the die is still completely filled by the material of the previous billet and their interaction produces a transition zone that extends to a variable length. The seam weld is generated in hollow profiles due to the material rejoining after the mandrel legs [5,6]; the charge weld is also generated at high hydrostatic pressure, but differently from the former, as it is usually contaminated by oxides, dust, or by lubricant received during loading into the press. While previous studies [7,8] have shown that seam welds, when the die design and the extrusion process are properly optimized, can

exhibit a mechanical resistance equal to that of base material, the whole profile length affected by the charge weld has to be discarded because of its lower mechanical proprieties. In order to do this, certain data are of critical importance: the position of the transition zone on the profile with respect to the stop mark, a permanent shape marker on the profile that indicates the end of a billet stroke, and its extent.

A number of works reported in literature investigated the charge welds phenomenon with the aim to evaluate the quality and the strength of the extruded profiles containing the transition zone [2, 9-17]. However, starting from the work carried out by Jonannes et al. [18], efforts have been also done in the experimental assessment of the charge welds extension to reduce the scrapped material. Jonannes et al. performed an extensive experimental work that showed how the material scrap can be reduced by changing the ratio of port volume to section cross section. Duplančić and Prgin [19] carried out a comprehensive investigation and a regression analysis on the effect of the temperature, degree of deformation, and height of the welding chamber on the charge weld length, but on a simple round tube with a fixed shape. In 2004, Jowett et al. [20] investigated nine hollow dies and four solid dies concluding that the flow in the ports should be balanced and that ports volumes should be reduced and designed proportional to the profile cross section in order to the reduce the scrapped material. However, as a further concluding remarks of the work, the paper reports that the ports reduction has two main drawbacks in the decrease of the press productivity and increase of the back-end defect. Pinter et al. [21] showed that the rule of volume reduction properly works, but for a tubular profile symmetrically fed. It then clearly emerges how an alternative solution to die design not only focused on ports volume variation should be determined to reduce the charge welds extend with the additional aim to not deteriorate the global process efficiency. Most recently, Yu et al.[14] proved that also the shapes of legs have greatly influences on the charge welds extension and that pointed legs produces shorter welds than those of the profile extruded with square legs.

A breakthrough in the understanding and prediction of the charge welds phenomenon and their extension has resulted from the use of numerical approaches. If experiments are expensive, time-consuming, and their conclusions can be drawn for a limited number of geometric configurations, numerical models allow one to investigate many different designs for a specific profile in a time well-matched to the industrial requirement. In the last decade, much work has been done on utilizing numerical approached to the extrusion process of aluminum profiles, which has been simulated by means of finite element (FE) codes [22-25]. However, the studies specifically dedicated to charge welds that employ numerical modeling tools are limited. Qiang et al.[26], Zhang et al.[16], performed FE simulations of charge welds phenomenon alloy by means of Lagrangian codes. The former investigated the formation and evolution of the transition zone at a very early stage of the process (less than 10 mm stroke); the latter focused the study on the oxide distribution at the interface with particular attention to oxides breakings during port filling and seam joining in welding chambers. Both investigations, however, utilized only 2D FE models and very simplified profile shapes due to the high computational cost of the Lagrangian approach, making a difficult task the extension of the results to more complex geometries. In addition, no experimental validation was performed in terms of charge weld formation and evolution. Later, Mahmoodkhani et al. [28] computed the thickness and length of the charge welds transition zone for different feeder dimensions and validated the calculation against industrial data, by still for a simplified 2D solid bar. In 2013, Reggiani and coworkers validated the capability of a commercial FE code to predict the charge weld extension for a complex 3D multi-hole porthole die, finding a good agreement between experimental and numerical data in terms of evolution of the phenomenon and dimensions of the segments to be discarded [29].

The aim of the present study was to investigate the way to minimize the front-end defect by a proper die design modification without affecting the overall process productivity for an industrial hollow profile made of AA6061 aluminum alloy. As a first step, the industrial experimental verification of the FE model use to predict the charge weld evolution for the initial die configuration was carried out. Then, the benefits

of an innovative die design, not only based on volume ports reduction but also on their shapes, were quantitatively evaluated by means of a numerical campaign both in terms of recovery and productivity, achieving a final optimized die design that allowed the extruder to consistently reduce the charge weld scrap. In addition, the sensitivity analysis of the results to process parameters (ram speed, billet temperature, and alloy) was also performed. Results were also compared, for the specific selected profile, with the theoretical prediction with the empirical model reported in literature in order to estimate charge weld extension for different die geometries. Jowett and coworkers [20] stated the validity of the simple rule that front-end weld scarp is to be equal to 1.5 times the total die volume divided by the profile cross section.

THE INTIAL DIE CONFIGURATION (DESIGN 1)

The selected starting die design configuration was a porthole die (Figure 1a), manufactured by Almax-Mori, Italy, with four cavities used to produce a hollow profile for light panels. The profile thickness (Figure 1b) was 5 mm for the bottom part of the profile and 6 mm for the upper one, and it presented two flat projections on the upper part of the profile with respect to the die positioning in press. The inner cavity of the profile was produced by a mandrel supported by four bridges, so that seam welding occurred, two in the middle of the horizontal long sides and two in the middle of the inclined ones. The section area of the profile was 2496 mm^2 and the maximum bearing length was 20.5 mm in the outer surface.

The ports of the die have been designed and manufactured with the aim of reducing the aluminum volume inside the porthole, thus reducing the charge weld extension. While doing so, the nest practices developed by Almax Mori have been used. The necessity to deliver the die in Indianapolis within two weeks from order did not give the authors the possibility of reducing the charge weld extension predicted by the first transient simulation.

(a)   (b)
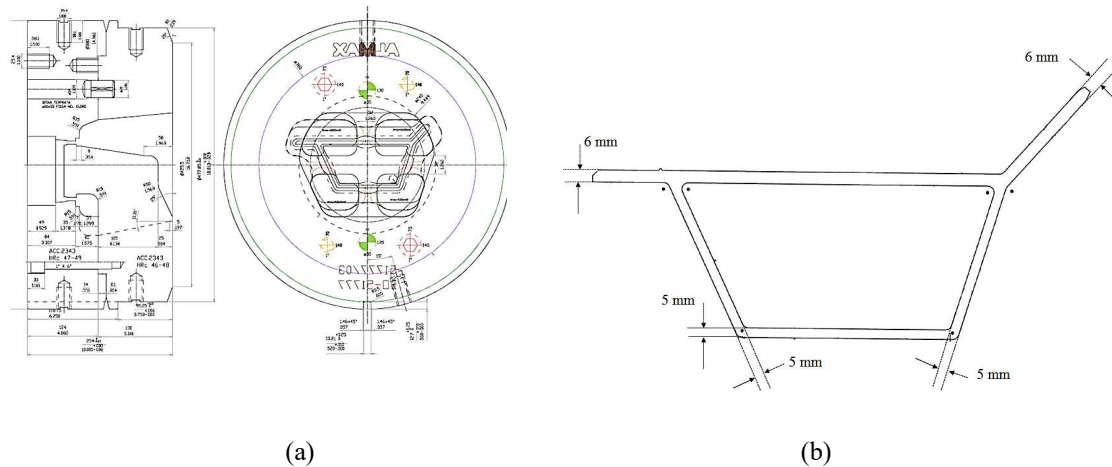
Figure 1. a) the die used in the experimental design with the profile labelling (press exit view) and **b)** profile shape.

FE MODEL EXPERIMENTAL VALIDATION FOR PREDICTION OF CHARGE WELD EVOLUTION

Experimental Set-Up and Results

The starting die configuration was experimentally used to manufacture and commercialize the profile made from a AA6061 alloy. The production was carried out on an industrial 3500 US ton extrusion press at the Alexandria Industries Midamerica plant with the aim of evaluating the die performances in terms of scrap minimization and to validate the FE model for the prediction of the charge weld evolution. This was done by accurately monitoring the first five consecutive billets and recording data in terms of billet length, preheating temperature, and peak process load. The first billet was a bit longer and hotter than the following billets in order to speed-up equilibrating the thermal regime. For the other fourth billets, the temperature of the container was kept at 420°C and that of the ram at 450°C. The die and the billet were both preheated at 480°C. Table 1 reports the initial thermal and geometrical conditions of the experimental set-up.

Table 1. Initial temperatures and geometries of the billets and tools involved in the experimental set-up.

	Temperature [°C]	Length [mm]	Diameter [mm]
Billets	480	673	265.0
Die	480	--	--
Container	420	1150	265.0
Ram	450	150	185.5

The transition between the 4th and the 5th extruded billets was chosen to investigate the welding phenomena interaction in order to be sure that the stationary conditions were achieved. The technique for sampling of coring is schematically illustrated in Figure 2. In detail, the front-end part of the extruded profile was analyzed by cutting 53 slices on the left side of the stop mark according to the techniques shown in Figure 3, which shows the extruded profiles and the labelling method used to track the sections of the profiles. Table 2 reports reported the length of the slices. Each specimen was ground and etched in Tucker's reagent (45 ml conc. HCl, 15 ml conc. HNO3, 15 ml 48% HF, 25 ml H_2O) [30] on the same side with respect to the extrusion direction. The etching time was selected to achieve a good visualization of the macrostructure and varied between 20 to 60 seconds per slice. The etched slices were then immediately observed by the unaided eye. For each slice, the percentage area of the new billet was computed by means of CAD software after scanned high resolution pictures of the etched specimens were acquired.

An example of the output result is reported in Figure 4 for the 14th slice where the new billet advancement is marked by the red areas. The profile clearly showed the "stop mark" thus allowing a stable position referencing in the several profiles independently of the process stroke. The charge welds appear after a certain length from the stop mark, after which the transition is complete and the profile is made of 100% new billet material. The analysis was carried out to determine the complete exhaustion of the charge welds. The exact position of the starting and ending point of the charge welds were then experimentally determined.

Rear Scrap	Sample	Good Metal → Extrusion Direction	Sample	Front Scrap

Figure 2. Experimental technique used to identify coring position in extrusions
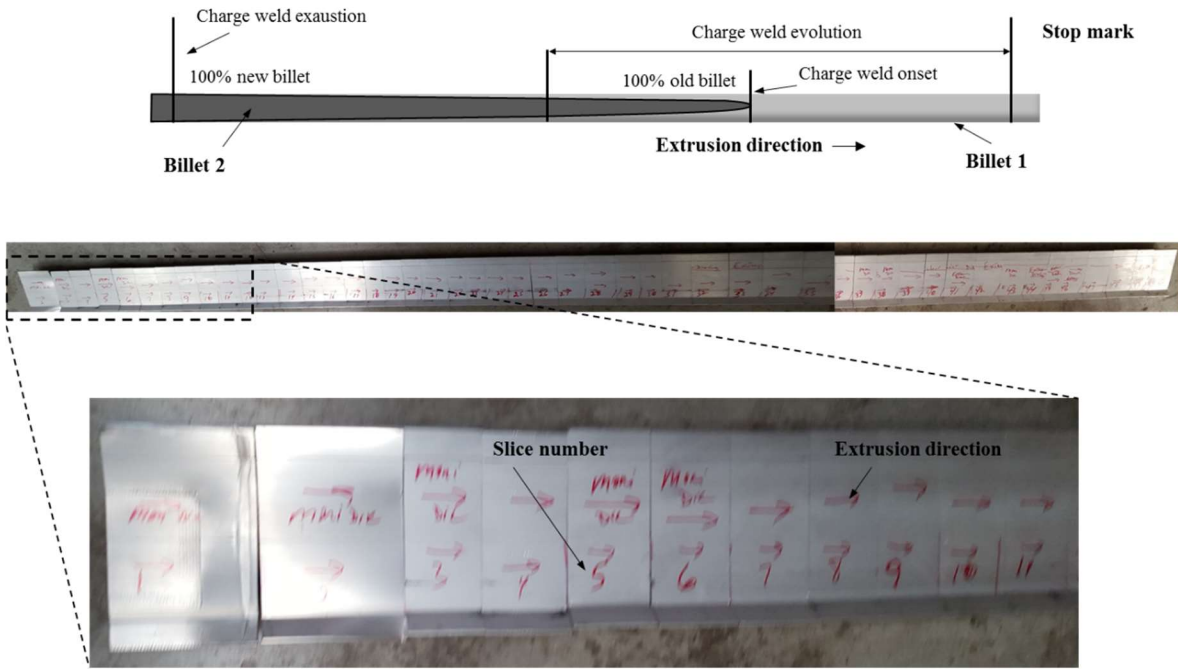
Figure 3. The extruded profiles of the fifth billet with stop mark evidence and the experimental sample labelling shown.

As can be observed from Figure 4, due to the presence of the die bridges, four billet-to-billet transition flows (charge welds) were generated that progressively converged towards the seam welds that were named X and Y for the flow in the upper part of the profile, and W and Z for those in the bottom part of the profile.

In Figure 5a the theoretical and experimental positions of the seam welds were examined. Welds emerged as light areas clearly visible in some of the etched slices. The shifting of the seam weld on the right oblique toward the upper part of the profile with respect to the position of the two bridges could be explained with a slower exit flow velocity of the flat projection, as can be observed in Figure 5b that plots a velocity map of the FE model. Concerning the left-side oblique seam weld, the reason of the shifting position with respect to the bridge was attributed to the increased extrusion ratio (thinner thickness) of the bottom part if compared to the upper one and then to the increased pressure (Figure 5c). Instead, the two vertical seam welds well matched with the expected positions on the bridges.
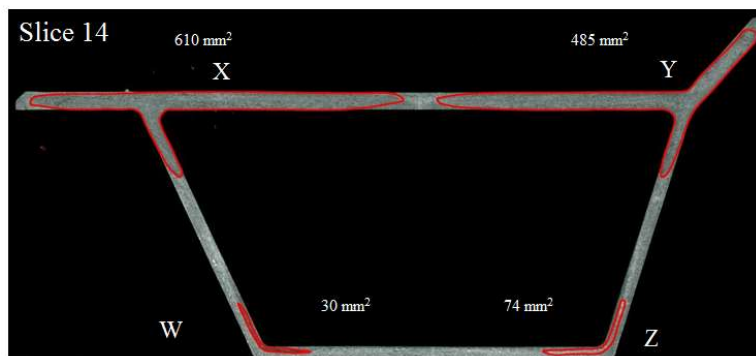
Figure 4: The acquired area of the four charge welds (X,Y,W,Z) for the 14th slice at a distance of 1378 mm from the stop mark.

Table 2. Experimental lengths of the cut slices.

Slice #	Length [mm]	Slice #	Length [mm]	Slice #	Length [mm]	Slice #	Length [mm]
1	145	15	82	29	83	43	114
2	150	16	90	30	74	44	98
3	85	17	86	31	98	45	75
4	97	18	74	32	122	46	109
5	97	19	79	33	106	47	115
6	95	20	73	34	125	48	118
7	97	21	100	35	105	49	80
8	87	22	68	36	76	50	116
9	82	23	75	37	95		
10	90	24	82	38	98		
11	90	25	86	39	108		
12	67	26	91	40	94		
13	95	27	98	41	125		
14	101	28	106	42	125		

(a)

(b)

(c)
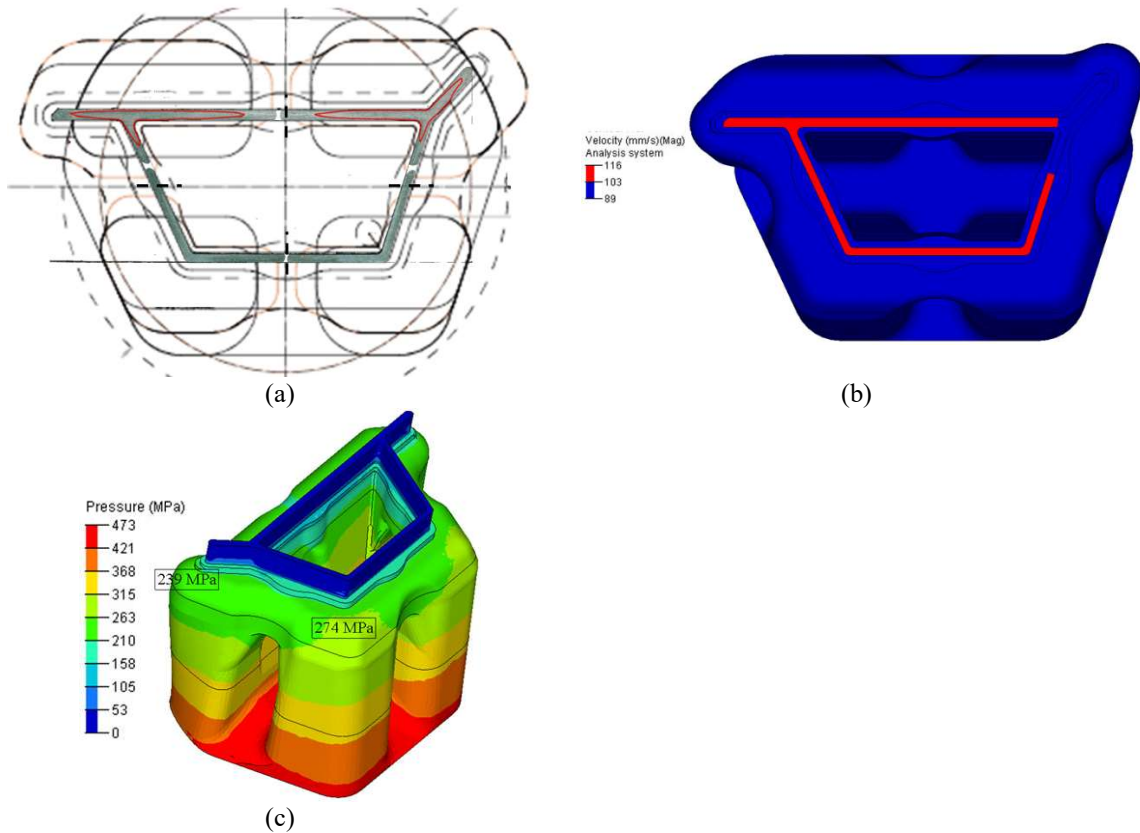
Figure 5. a) position of the four bridges in the die (dotted line) and of the experimental seam welds (light areas) with the area of the new billet progress also visible (red areas) for the slice 12 at a distance of 1182 mm from the stop mark, **b)** FE simulation results in terms of profile exit velocity [mm/s] and, **c)** pressure map [MPa].

In Figure 6, four steps of the experimental evolution of the charge welds in the profile at increasing distance are shown. Figure 6a and 6b show 4% and 32% respectively of the old material replacement with the new billet that appears as two small closed loops on the uppers side of the profile (X, Y flows), the thicker side. The Y flow is only in a slight delay compared to the X flow; indeed, at slice 11, the measure of the X and Y flow area is almost the same, i.e., 402 mm^2 and 383 mm^2, respectively. As can be seen, both flows (X, Y) converge to the central seam weld with the same velocity. The third flow (Z flow) emerged from the right-bottom part, immediately followed by the W flow (Figure 6c) when the thicker upper part was not completed yet. It is well apparent in Figure 6d that at slice 33 there is almost no residual trace of charge weld in the profile.

(a) SLICE 9, 0.935 MT FROM THE STOP MARK 4% OF OLD MATERIAL REPLACEMENT

(b) SLICE 11, 1.2 MT FROM THE STOP MARK 32% OF OLD MATERIAL REPLACEMENT

(c) SLICE 15, 1.46 MT FROM THE STOP MARK 59% OF OLD MATERIAL REPLACEMENT

(d) SLICE 33, 3.0 MT FROM THE STOP MARK 98% OF OLD MATERIAL REPLACEMENT
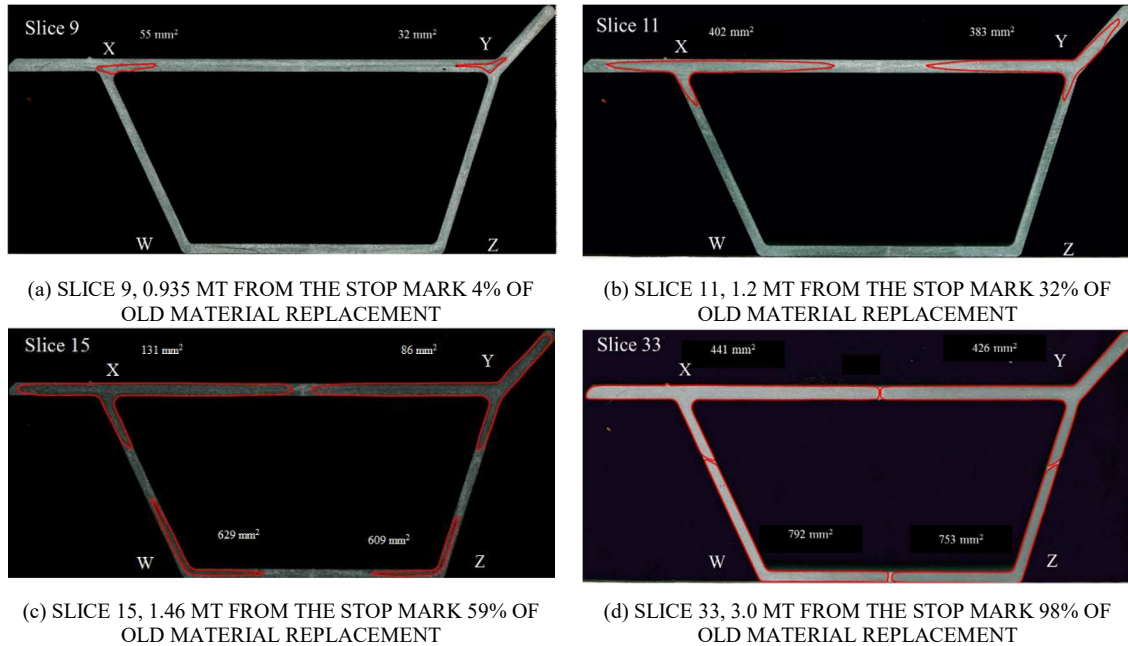
Figure 6. Experimental charge weld evolution on the profile: image analysis of the profile at increasing distance from the stop mark.

The Finite Element Model

The evolution of the charge welds was simulated in the investigated extruded profiles by means of a commercial FE code used for the analysis and optimization of the extrusion process and dies, based on a fluid dynamic approach for modelling incompressible flows, including non-Newtonian fluid behavior. In such an approach, the model of the aluminum billet had to resemble the final shape of the extruded profile (Figure 7a). The bearing curves were extracted by the 3D CAD model of the die and then projected on the billet surfaces (Figure 7b).

(a)   (b)
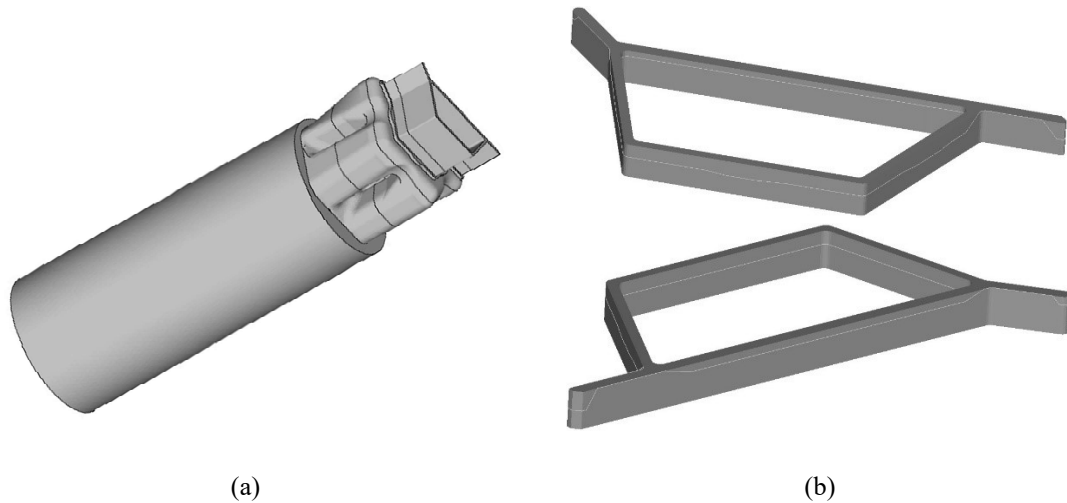
Figure 7. a) The 3D CAD model of the billet and **b)** magnification of the bearing curves.

The profile did not present any symmetry so that the complete profile was modelled. The resulting model was divided into 7 components due to the different boundary conditions and mesh refinement involved: billet, feeder, porthole, pocket 1, pocket 2, bearings, and profile (Figure 8). The computation of the charge weld evolution did not require the simulation of the tools that, for this reason, were not included in the model. However, the heat exchange at the tool-billet interfaces was accounted for by setting proper values of the convective coefficients and reference temperatures.
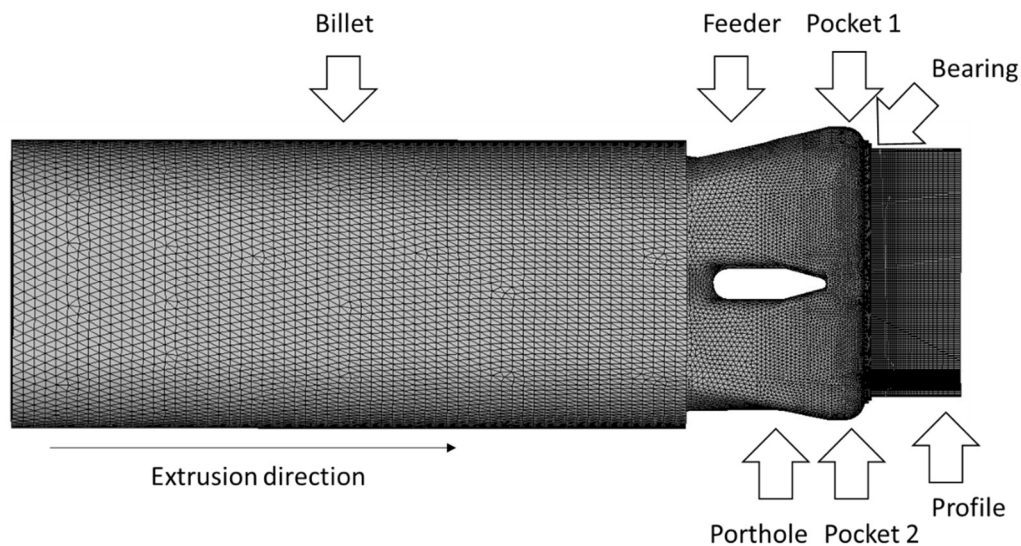
Figure 8. FE model of aluminum with the defined components.

The billet and porthole components were free meshed with 3D tetrahedral 4-noded elements. Due to the higher accuracy required in the bearing and profile regions, 3D prismatic 6-noded elements were used for these regions. The final model consisted of 885090 elements. The initial temperature of the billet in the FE simulation was set equal to the last recorded temperature before the loading into the press (i.e., 480°C). A ram speed of 5 mm/s was set in the simulation, producing a mean profile speed of 107 mm/sec.

At the two exits, a zero normal stress boundary condition was specified. A full sticking condition was set all around the billet surfaces except on the bearings where a visco-plastic friction model with a coefficient value of 0.3 was used, accounting for the material sliding that occurs in these regions. A convective coefficient of 3000 W/m²-°C was set between aluminum and the tool system (container, die, and ram), while the initial temperatures of the tools were used as reference temperatures. Heat flux was set equal to zero for the free surface condition at the profile surfaces. The ram speed was imposed by applying the prescribed velocity at the billet back. The effective flow stress of the AA6061 alloy was expressed by the Hansel and Spittel formulation with eight parameters optimized by the authors by means of torsion testing.

The weld length calculation was performed by means of a transient analysis with moving boundaries. In this type of problem, the boundary conditions for the flow and heat transfer equations are treated as time-dependent and the position of the billet back and of the billet-container interface are tracked during the simulation time. The mesh in the profile, bearing, porthole and welding chamber remain fixed, but in the billet region the elements scale down linearly in the extrusion direction at each time step. A variable number of time steps was defined according to the experimental length of the cut slices. The total simulation time for a single transient run was 12.7 hours.

In Figure 9 the evolution of the transition between the new (red) and the old (blue) billets at four progressive time steps is reported. The FE code correctly predicted the replacement of the billet that first affected the thicker upper (X and Y) of the profile (steps 9 to 12) and then the thinner bottom part (W and Z) (from step 13).

(a) Step 9 – time 8.1 sec

(b) Step 11 – time 9.9 sec

(c) Step 15 – time 13.5 sec

(d) Step 19 – time 17.1 sec
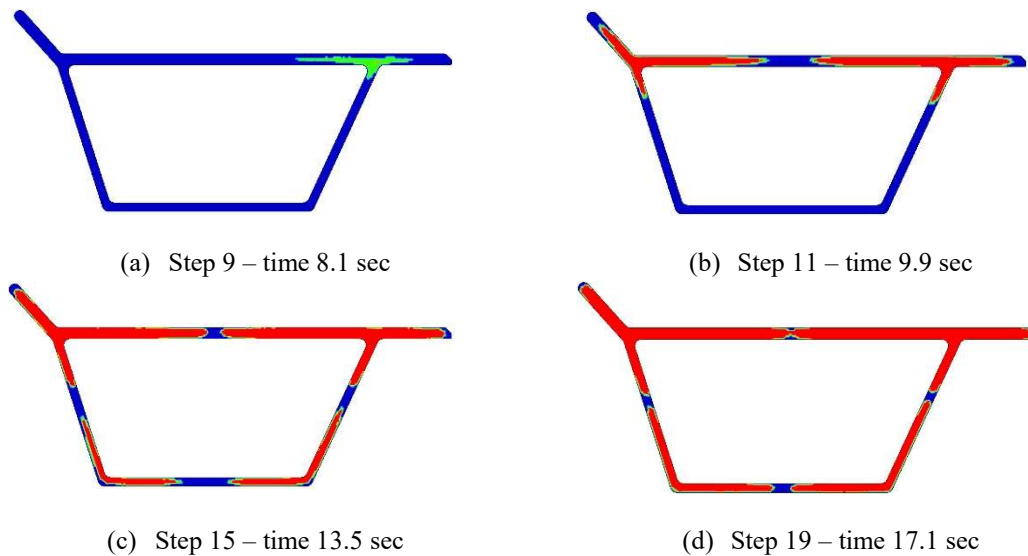
Figure 9. Evolution of the transverse weld at various subsequent time steps.

Comparison of Experimental and Numerical Results

Figure 10 shows the comparison of the percentage of the billet replacement over the stop mark distance as experimental and numerical predicted. As can be seen, a very good agreement was found between simulation and experiment, both in terms of charge weld length (starting and exhausting points) and general trend.
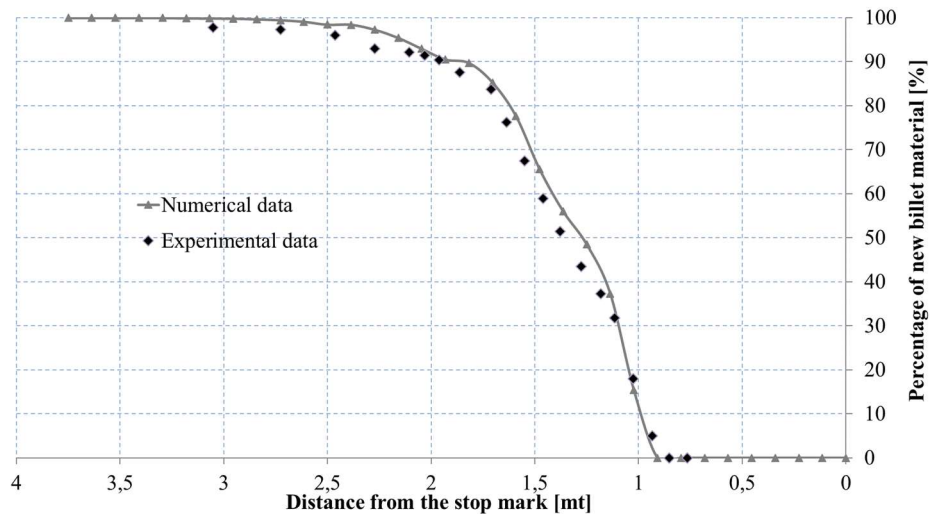
Figure 10. Comparison of the experimental *vs*. numerical results for percentage of new material over the stop mark distance for the investigated profile.

EVALUATED DIE AND PROCESS DESIGN MODIFICATIONS

The main objective of the present work was to minimize the front-end defect without affecting the productivity of the hollow profile extrusion. For this, the challenge was to optimize the balance of the ports to the profile area without compromising the flow balance and, in addition, without disregarding the restrictions specified by the end user, as the position of seam welds.

The purpose of proportioning the port volumes to the areas they are feeding was to obtain similar charge weld lengths for different ports, thus increasing the recovery. In order to reach this target one can proceed in different ways. In case of the structural hollow profile examined in this paper, the authors considered the following best practices while designing the die:

- Avoid seam welds on the profile areas effected by milling or welding
- Guarantee a superior seam weld quality
- Guarantee the ram velocity specified by Alexandria Industries Midamerica (extruder)
- Reduce the volume of aluminum filled in the die by minimizing the dead metal flow

Last, but not least, is the practice that the authors developed in the last five years thanks to FE analyses and evidences collected on industrial presses.

At the end of the work, two alternative die configurations were generated and numerically investigated, in the following named DESIGN 1 (initial die configuration), DESIGN 2, DESIGN 3. The same settings previously described for the initial configuration were adopted for each generated model. With the aim to better understand the design criteria selected to move from one design to the other, according to what reported in literature by Jowett et al. [20], each of them were analytically investigated in terms of port volumes, profile areas, FE analysis estimation of charge weld lengths and empirical estimation of charge weld lengths on the basis of the formula suggested in literature [20]. Due to the symmetry, no distinction was made between the upper ports A and B and between the lower ports C and D so that their sum was therefore accounted for in the discussion.

DESIGN 1
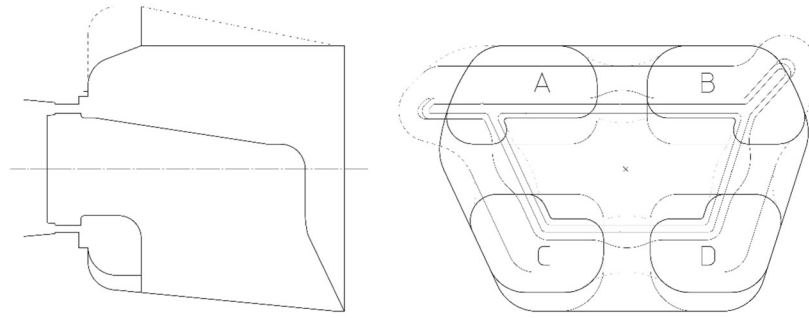
Figure 11. Ports layout and two main sections for DESIGN 1 (initial die configuration)

Port Number	Port Volume [mm3]	Profile Area [mm2]	Ratio Volume /Area	Charge Weld (FEM) [mm]	Charge Weld empirical [20] [mm]
A+B	2.20 e6	1678	1311	-	1967
C+D	1.83 e6	896	2042	-	3064
Total	4.05 e6	2574	1573	2750	2360

Table 3. Port volumes, profile areas, FE analysis estimation of charge weld lengths, empirical estimations of charge weld lengths for DESING 1.

From Figures 6,9 and Table 3 it was clear that, for the DESIGN 1, the lower die ports (C+D) showed a longer extension of the charge welds (2042 mm) than the upper ports (A+B) (1311 mm). In order to reduce the extension of the charge welds, according to what previously reported in literature [20], as first design step, the volumes of ports C and D was reduced with the specific aim to decrease the local ratio between ports volumes and profile fed area. As a result, the DESIGN 2, shown in Figure 13, was generated by imposing a "cylindrical" reduction of ports C and D. However, as reported in Table 3, 4 and synthetically shown in Figure 17, this modification produced an increase in the scrapped material moving from 2750 mm of the transition zone in DESIGN 1 to 3160 mm of the DESIGN 2. This is in contrast with what expected from the computation of the charge weld extension according to the empirical formula reported in literature [20] that predicted a longer transition for the DESIGN 1 (last column in Tab. 3 and 4). It comes clear from Figure 13 that the C and D ports volume reduction led to a decreased replacement velocity for the shorter side of the profile (upper figures in Fig. 13a,b,c) and, at the same time, to an increased replacement for the longer sides (bottom figures in Fig. 13a,b,c). This result is also visible in Figure 16 (upper) that shows the flow velocity for the three investigated geometric configurations; it is well evident the significant flow unbalance for the DESIGN 2 that would also lead to a decrease in the process productivity so coming in contrast with one of the specific design constraints. This worsened result was achieved even if the ratio of volume to area for flows of A+B was more balanced to that of C+D ports in DESIGN 2 than in DESIGN 1 (1311 to 2042 for DESISGN1 and 1274 to 1659 for DESIGN 2). In other words, from Figure 13 it can notice the effect of DESIGN 2 and 3 on the dead metal flow; DESIGN 3 was the one with lowest percentage of dead metal flow

despite port volume C+D was similar to DESIGN 2. The dynamic compression of DESIGN 3 was allowing the minimization of the dead metal flow.

DESIGN 2
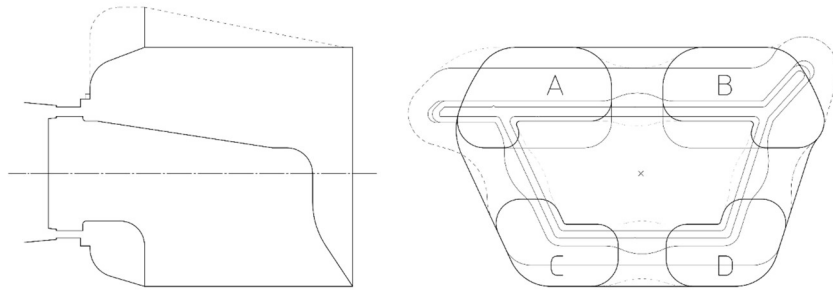
Figure 12. Ports layout and two main sections for DESIGN 2 with ports C and D cylindrically reduced in volume if compared to DESIGN 1.

Port Number	Port Volume [mm3]	Profile Area [mm2]	Ratio Volume /Area	Charge Weld (FEM) [mm]	Charge Weld (empirical) [20] [mm]
A+B	2,22 e6	1742	1274	-	1912
C+D	1,38 e6	832	1659	-	2488
Total	3,60 e6	2574	1399	3160	2098

Table 4. Port volumes, profile areas, FE analysis estimation of charge weld lengths, empirical estimation of charge weld lengths for DESING 2.

With the aim to speed up the flow in ports C and D while maintaining a balance with that in ports A and B, as next step of work a third configuration was designed (DESIGN 3) (Figure 14) with a "conical" reduction of the ports C and D if compared to DESIGN 1 but with almost the same volumes as in DESIGN 2. Detailed information on DESIGN 3 are reported in Table 5. If the computed charge welds length for the DESIGN 3 is compared to that of DESIGN 2 (2640 mm to 3160 mm), the influence of the ports shape clearly emerged. One of the consequence of the ports reshaping was also the re-dimensioning of the welding chamber that maintained the height but reduced the width, with a benefit also in terms of pressure (Fig. 15) and seam weld quality (Fig. 16) [21]. It can be concluded that it is not a matter of port volume reduction only, as the shape of the modified ports has a major effect on the reduction of the local charge weld extension for ports C and D. This is due to the fact that DESIGN 3 maintains the same ports volume C and D of DESIGN 2 while increasing the lead-in area, thus avoiding the reducing of the profile area section fed as happened in in DESIGN 2. The success of DESIGN 3 in respect of DESIGN 2 is therefore due to the shape of the port and not on its volume.
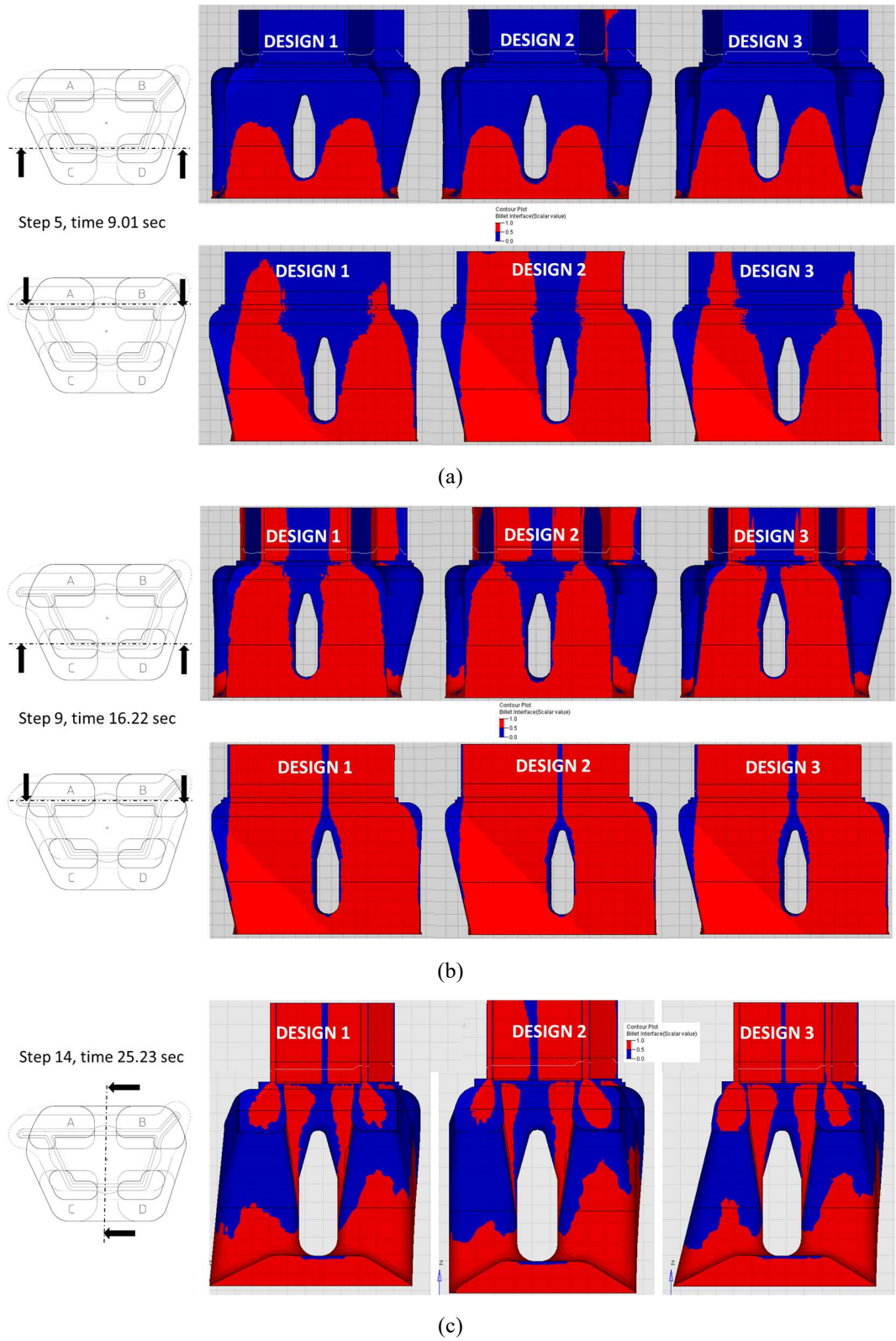
Figure 13. Billet replacement (blue= old billet, red= new billet) for the three evaluated designs (from left to right: DESIGN 1, DESIGN 2 and DESIGN 3) and three subsequent simulation steps (a,b,c). Three different aluminum sections are shown.

It is also interesting to compare the billet replacement for three subsequent simulation steps for each evaluated design (Figure 13). Even if in DESIGN 3 the flow in ports A and B (feeding the longer side of the profile) was slowed down in comparison with DESIGN 2 (Fig. 13a,b bottom) while that of the shorter side was speed-up (Fig. 13a,b upper), the global effect was a more balanced replacement at the die exit (Fig. 13c). In addition, the material scrap was reduced form 2750 mm of the DESIGN 3 to 2640 mm of the DESIGN 1. The empirical formula reported in [20] was found in contrast also with the numerical evidences of DESIGN 3.
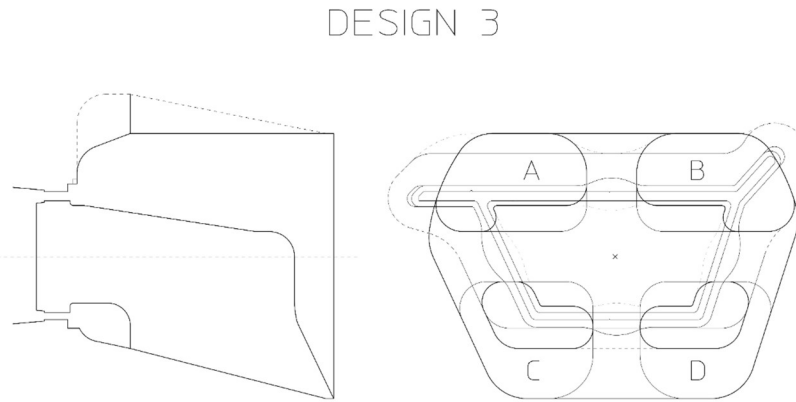
DESIGN 3

Figure 14. Ports layout and two main sections for DESIGN 3 with ports C and D conically reduced with the same volume of DESIGN 2.

Port Number	Port Volume [mm3]	Profile Area [mm2]	Ratio Volume /Area	Charge Weld (FEM) [mm]	Charge Weld (empirical) [mm]
A+B	2,21 e6	1716	1288	-	1932
C+D	1,44 e6	858	1678	-	2517
Total	3,65 e6	2574	1418	2640	2127

Table 4. Port volumes, profile areas, FE analysis estimation of charge weld lengths, empirical estimation of charge weld lengths for DESING 3.

In Fig. 17 the evolution of the charge welds for DESIGN 1, 2 and 3 over the stop mark distance is reported. The detrimental effect of the DESIGN 2 if compared to the alternative die configurations appears.

A sensitivity analysis was additionally carried out by means of transient simulations in order to evaluate the effect process parameters on charge weld extension. To this aim, with respect to the initial die design settings (5 mm/s of ram speed, AA6061, 480°C of billet preheating), the ram speed, the alloy and the billet preheating temperature were varied once a time. The geometric configuration of DESIGN 1 was adopted in each run. In detail, a ± 50% of the ram speed was investigated so that a two simulations were run with a prescribed ram velocity of 3 and 7 mm/s. Then, two simulations were set with a different extruded alloy defined according to the Hansel Spittel law, the AA6063 and AA7020. Finally, with a ram speed of 5 mm/s and an extruded alloy AA6063, the billet preheating temperature was varied from 460°C and 490°C. Results were compared in terms of charge weld evolution and are summarized in Figure 18. As can be seen, the charge weld extension

was not influenced by the main process parameters and by the aluminum alloy extruded, thus confirming what previously reported in literature based on experimental activities [19].
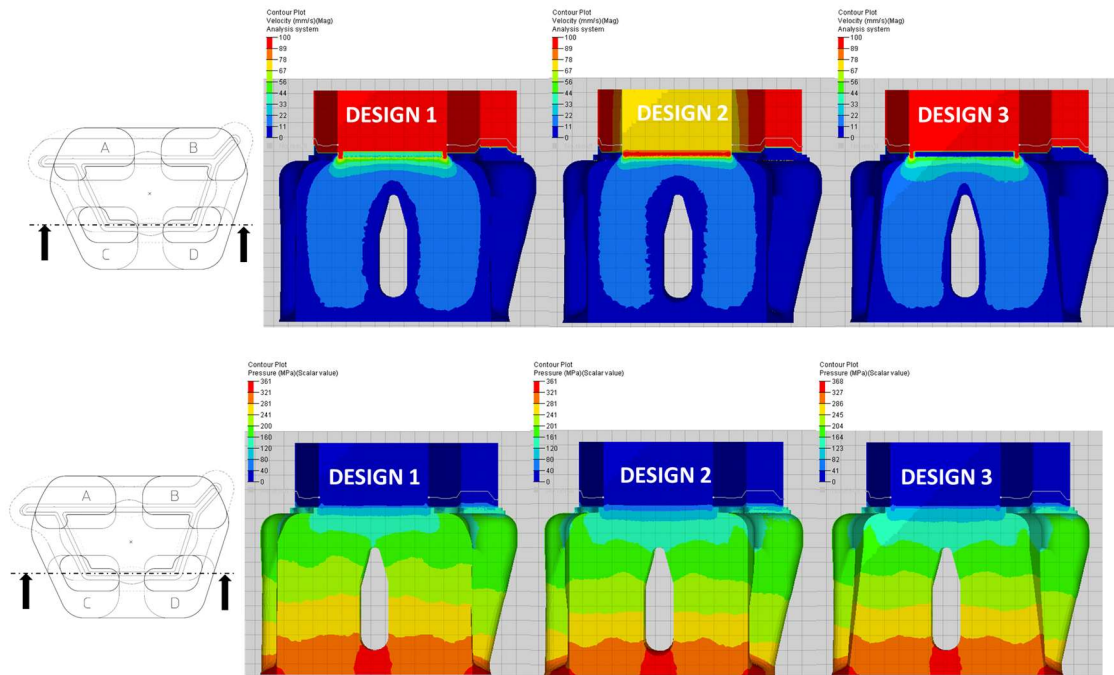
Figure 15. Upper- Numerical flow velocity field [mm/s]. Bottom- pressure map [MPa]
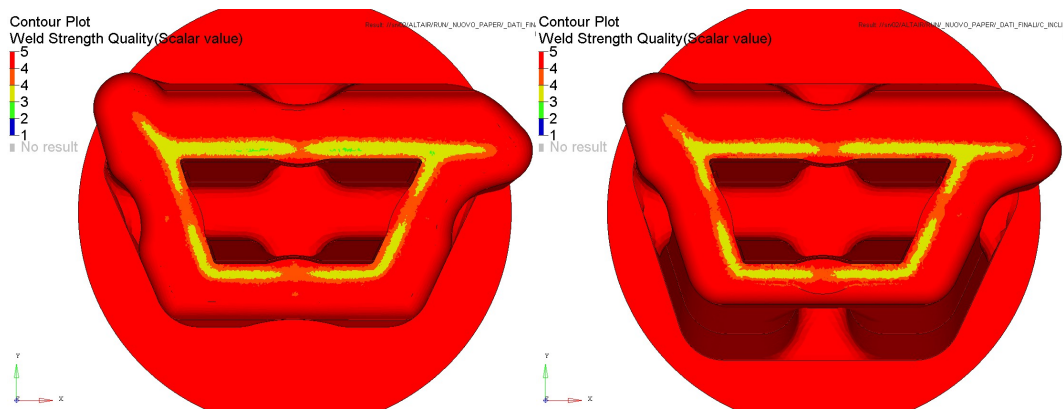
Figure 16. Comparison of seam weld quality for DESIGN 2 (left) and DESIGN3 (right) by means of FE code criteria.
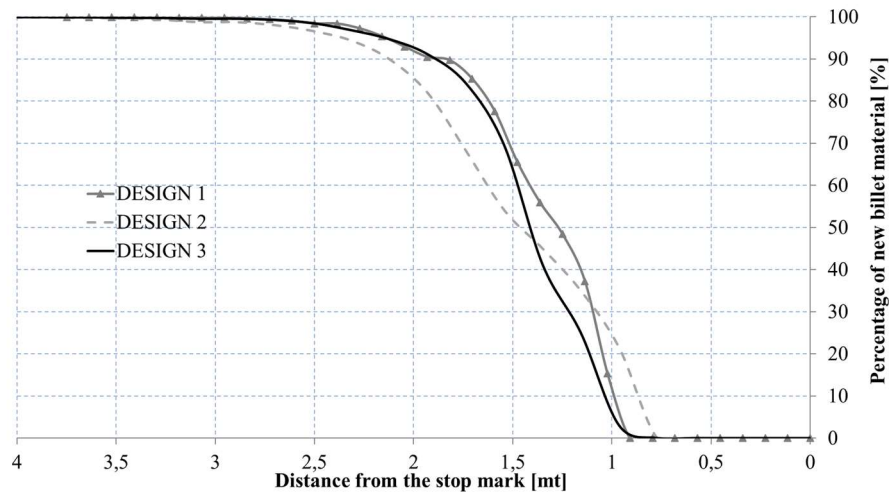
Figure 17. Evolution of the charge weld over the stop mark distance for DESIGN 1, 2 and 3.
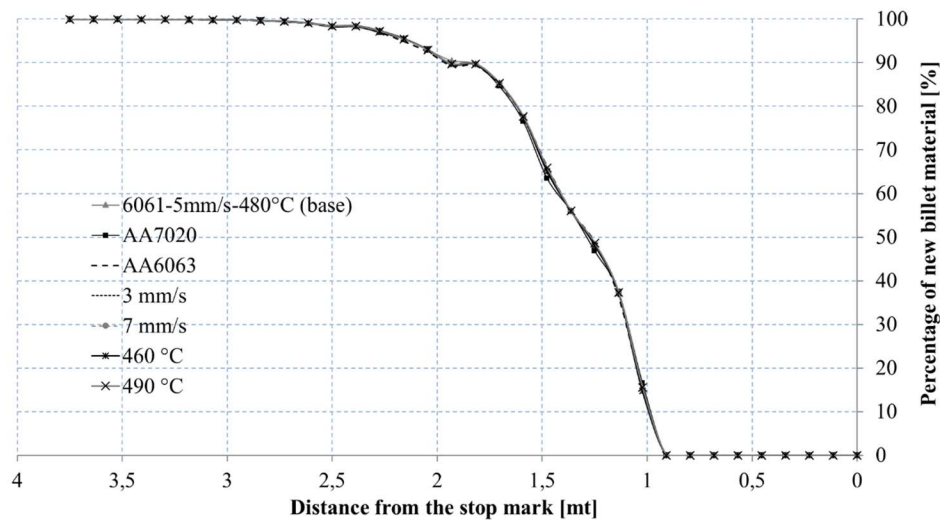
Figure 18. Charge weld extension as a function of die geometry and extrusion process parameters.

CONCLUSIONS

The main objective of the job presented in this paper was to minimize the front-end defect without affecting the productivity of the hollow asymmetrical profile extrusion. While engineering a porthole die required to extrude a structural profile, despite the restrictions specified by the end user, e.g., position of seam weld, it was possible to better balance the ports to the profile area they are feeding without compromising the flow balance. In summary, the following conclusion were drawn:

- FE analysis was found to be an accurate tool for the assessment of the charge weld extension in direct extrusion of hollow profiles.
- The material scrap reduction was demonstrated to be not only a matter of port volume reduction but it was also strongly influenced by the ports shape.
- A cylindrical reduction of the ports volume for an asymmetrical profile led to an increase in both the flow unbalance and charge weld extension.

- The dynamic compression of the flow in conical ports, without altering the global volume, resulted in a lower transition zone.
- Empirical formulas reported in literature were not suitable to predict the amount of material scrap.
- The charge weld extension and pattern, as numerical predicted by the FE code, was not influenced by the main process parameters (ram speed and billet preheating temperature) and by the extruded aluminum alloy.

REFERENCES

1. Parson, N.C., Hankin, J.D., Bryant, A.J., 1992. The metallurgical background to problems occurring during the Extrusion of 6XXX alloys. Proc. of the 5th International Aluminum Extrusion Technology Seminar, Chicago, USA, Vol. II, 13-24.

2. Akeret, R.,1992. Extrusion Welds-Quality Aspects are now centre stage. In the Proc. of the 5th ET Seminar, vol II, 319-336.

3. Lefsta, M., Reiso, O., Johnsen, V., 1992. Flow of the billet Surface in Aluminum Extrusion. In the Proc.of 5th International Aluminum Extrusion Technology Seminar, Chicago, USA, vol II, 503-518.

4. Valberg, H., 1988. Physical Simulation of Metal Extrusion by Means of Model Materials. In the Proc. of 4th International Aluminum Extrusion Technology Seminar, Chicago, USA, vol II, 321-328.

5. Valberg H., 2002, Extrusion welding in aluminium extrusion,Int. J. of Materials & Product Technology, 17/7, 497-556.

6. Bariani P.F., Bruschi S., Ghiotti A., 2006, Physical simulation of longitudinal welding in porthole-die extrusion, CIRP Annals-Manufacturing Technology 55(1), 287-290.

7. Donati, L., Tomesani, L., Minak, G., 2007. Characterization of seam weld quality in AA6082 extruded profiles. Journal of Materials Processing Technology 191, 127–131.

8. Nanninga N., White C., Mills O., Lukowski J., 2010, Effect of specimen orientation and extrusion welds on the fatigue life of AA6063 alloy, International Journal of fatigue 32, 238-246.

9. Sheppard T., 1999. Extrusion of aluminum alloys. The Netherlands: Kluwer Academic Publisher, 1999.

10. den Bakker, A.J., Katgermanc, L., van der Zwaag, S. 2016. Analysis of the structure and resulting mechanical properties of aluminium extrusions containing a charge weld interface. Journal of Materials Processing Technology 229, 9–21.

11. den Bakker, A.J., Sillekens, W.H., Werkhoven R.J., 2008. Experimental study of longitudinal weld-seam properties in tubular AA6060 and AA6082 extrusions. In the Proceedings of the 9th International Aluminum Extrusion Seminar & Exposition, (ET), Orlando FL, USA.

12. Laue K., Stenger H., 1981. Extrusion. Ohio: American Society for Metals, Metal Park, 4073.

13. Ren, X. Zhang, J. L., Li, J. P., 2015. Microstructural Characterization of Extrusion Welds in 6xxx Aluminum. In the Proceedings of the 3rd International Conference on Material, Mechanical and Manufacturing Engineering (IC3ME), 1857-1863.

14. Yu, J., Zhao G., Chen L., 2016. Investigation of interface evolution, microstructure and mechanical properties of solid-state bonding seams in hot extrusion process of aluminum alloy profiles. Journal of Materials Processing Technology 230, 153–166.

15. Zhu JH, Young B, 2007. Effects of transverse welds on aluminum alloy columns. Thin-Walled Struct 45(3), 321–329.

16. Zhang X, Feng D, Shi X, Liu S, 2013. Oxide distribution and microstructure in welding zones from porthole die extrusion. Trans Nonferrous Met Soc China 23(3):765–772

17. Kandis, J., 2013. New method for quality inspection of extrusion welding. PhD thesis of the Riga Technical University, Institute of Mechanical Engineering Technologies.

18. Jonannes VI., Jowett, CW, Dickson, RF., 1996. Temperature distribution in aluminum extrusion billets. In the Proceedings of the 6th International Aluminum Extrusion Technology Seminar vol. 2, Chicago, Illinois, USA, 89-94.

19. Duplanĉić I., Prgin J., 1988. Material flow in the extrusion of hollow aluminum sections, through hollow dies. In the Proc. of 4th International Aluminum Extrusion Technology Seminar, Vol. 2, 235–240

20. Jowett C., Adams J., Daughetee C., Lea G., Huff O.A., Fossl, N. 2008. Scrap Allocation. In the Proceedings of the 9th International Aluminum Extrusion Seminar & Exposition, (ET), Orlando FL, USA, 13-16.

21. Pinter, T., Reggiani, B., Donati, L., Tomesani, L., 2015. Numerical Assessment of the Influence of Process and Geometric Parameters on Extrusion Welds and Die Deformation after Multiple-cycles. Materials Today: Proceedings 2 (10), Part A, Aluminium Two Thousand World Congress and International Conference on Extrusion and Benchmark ICEB 2015, 4856–4865.

22. Reggiani, B., Donati, L., Tomesani, L., 2010. Effect of different FE simulation codes in the stress analysis of extrusion dies. In the Proc. of the 13th International ESAFORM Conference on Material Forming, University of Brescia, Brescia, Italy, 7-9 April.

23. Sommitsch, C., Sievert, R., Wlanis, T., Günther, B., Wieser, V., 2007. Modelling of creep-fatigue in containers during aluminium and copper extrusion. Computational Materials Science, 39, 55–64.

24. Tomesani, L., Reggiani, B., Donati, L., Khalifa, N.B., Tekkaya, A.E., 2010. Experimental evaluation and numerical analysis of speed-related effects in aluminium extrusion. In the Proc. of the 60th CIRP, Accademia Internazionale di Ingegneria della Produzione (http://www.cirp.net), 22nd-28th August, Pisa, Italy.

25. Zhou, J., 2003. 3D FEM simulation of the whole cycle of aluminium extrusion throughout the transient state and the steady state using the updated Lagrangian approach. J. Mater. Proc. Technol., 134, 383-397.

26. Qiang L, Harris C, Jolly MR, 2003. Finite element modelling simulation of transverse welding phenomenon in aluminium extrusion process. Mater Des 24–7:493–496

27. Zhang C, Zhao G, Chen H, Guan Y, Kou F (2012) Numerical simulation and metal flow analysis of hot extrusion process for a complex hollow aluminum profile. Int J Adv Manuf Technol 60:101–110

28. Mahmoodkhani Y, Wells M., Parson N., Jowett C., Poole W., 2014. Modeling the formation of transverse weld during billet-on-billet extrusion. Materials 7, 3470-3480.

29. Reggiani, B., Donati, L., Tomesani, L., 2013. Prediction of charge welds in hollow profiles extrusion by FEM simulations and experimental validation. International Journal of Advances Manufacturing Technologies 69 (5), 1855-1872.

30. George F. Vander Voort, Asm Metals Handbook Volume 9 - Metallography and Microstructure.